Bulletin of the Seismological Society of America, Vol. 99, No. 6, pp. 3454–3469, December 2009, doi: 10.1785/0120080330

# Estimation of the Breakdown Slip from Strong-Motion Seismograms: Insights from Numerical Experiments

by Víctor M. Cruz-Atienza,* Kim B. Olsen, and Luís A. Dalguer†

**Abstract** Fukuyama and Mikumo (2007) presented a method to extract information about the friction controlling earthquake rupture directly from near-field seismograms recorded out to several kilometers from a fault. This method computes a parameter ($D_c''$) approximating the breakdown slip ($D_c$) from the rake-parallel displacement at the time of the peak particle velocity. The validation of the method was based on simple 2D steady-state Green's functions, an approach lacking sufficient physics of the rupture process to support their conclusions. Here, we use 3D simulations of subshear strike-slip spontaneous rupture propagation to demonstrate that $D_c''$ is almost always controlled by rupture and wave propagation effects, rather than the fault friction process. Only if rupture reaches the Earth's surface and within a short distance from the fault ($R_c$) is it possible to extract information about $D_c$ from strong-motion data, due to the fast decay with distance from the fault of the seismic energy related to the stress breakdown process. Beyond $R_c$, $D_c''$ is controlled by the dynamic stress drop from the earthquake rupture without information about $D_c$. $R_c$ is comparable to the length of the fault cohesive zone where the breakdown process takes place during rupture and approximately equal to 80% of the wavelength associated with the breakdown frequency, defined as the reciprocal of the time span required by the stress to drop to the dynamic level. Our findings suggest that the $D_c$ estimate by Fukuyama and Mikumo (2007) for the 2000 $M_w$ 6.6 Tottori earthquake is unrelated to the breakdown slip. Moreover, the very narrow widths for $R_c$ obtained from our simulations are in agreement with previous studies challenging the resolution of bandlimited strong-motion data to estimate $D_c$ from kinematic-rupture models (Guatteri and Spudich, 2000; Spudich and Guatteri, 2004).

## Introduction

Our limited knowledge of the dynamic constitutive behavior of faults at seismogenic depths for large earthquakes has been a tremendous limitation in the investigations of the physical processes involved in fault rupture. Laboratory experiments have been our main source of such information, providing important insight into the nature of the constitutive laws that govern the interface sliding during earthquakes, represented as friction models (e.g., Dieterich, 1979; Ruina, 1983; Ohnaka *et al.*, 1987). Based on these laboratory experiments (admittedly performed at much smaller spatial scales than those characteristic for real earthquakes), simplified friction models have been proposed to study earthquake behavior in nature. However, the limited information available from the laboratory experiments has challenged Earth scientists to search for field observations to help parameterize the friction models. In particular, the linear slip-weakening friction model (Ida, 1972; Palmer and Rice, 1973; Andrews, 1976), characterized by the breakdown slip $D_c$, has been used in many different studies to investigate earthquakes. For example, Ide and Takeo (1997) used results from waveform inversion of strong-motion records obtained during the 1995 Kobe earthquake and found that $D_c$ ranges between 50 and 100 cm for deeper fault sections and between 100 and 150 cm for shallower fault sections. Since the pioneering work by Ide and Takeo, several studies have attempted to estimate $D_c$ from kinematic analysis of fault ruptures (e.g., Pulido and Irikura, 2000; Mikumo and Yagi, 2003; Miyatake *et al.*, 2004; Yasuda *et al.*, 2005). These studies were faced with a serious problem related to the strong influence on $D_c$ estimates from the slip functions assumed in their procedures (Piatanesi *et al.*, 2004).

However, the most delicate issue related to the estimation of $D_c$ from kinematic source analysis seems to be the

*Now at Departamento de Sismología, Universidad Nacional Autónoma de México.

†Now at Institute of Geophysics, ETH-Zurich, CH-8093 Zurich, Switzerland.

resolution of the stress breakdown process (Guatteri and Spudich, 2000). For instance, it has been shown that limited-bandwidth seismograms used to image the fault slip history may bias the estimates of $D_c$ (Spudich and Guatteri, 2004) in exactly the same way this parameter behaves on real earthquakes, where it seems to correlate with the final slip (e.g., Mikumo and Yagi, 2003; Mikumo *et al.*, 2003; Zhang *et al.*, 2003). In fact, when using off-fault ground-motion records to constrain $D_c$, it is difficult to determine whether the periods generated during the breakdown process are present in the recorded seismograms. These periods may not be present due to either low-pass filtering from postprocessing or spatiotemporal smoothing due to wave and rupture propagation effects primarily affecting high frequencies (e.g., Madariaga, 1978; Anderson and Luco, 1983; Dunham and Archuleta, 2005). The periods related to $D_c$ correspond to the breakdown times, $T_c$, which are the time spans required for the shear stress to decrease from its peak value to a dynamic stress level on the fault (Ohnaka and Yamashita, 1989). Thus, resolving $D_c$ on the fault plane through any method based on observed seismograms requires that the ground-motion spectra are sufficiently broad to contain frequencies higher than or equal to those given by the breakdown times $T_c$ (Guatteri and Spudich, 2000).

Mikumo *et al.* (2003) introduced a method to estimate $D_c$ on the fault plane as the slip at the time of the peak slip rate ($D_c'$). Based on this work, Fukuyama and Mikumo (2007, hereafter referred to as F&M) proposed to extend this method beyond the fault plane by estimating a parameter, here referred to as $D_c''$, directly from near-fault seismograms. F&M defined $D_c''$ as twice the rake-parallel free-surface displacement at the time of the peak particle velocity, where the factor of 2 arises from the assumption of an equal amount of opposite displacement on either side of the fault. They concluded that the method provides reliable $D_c''$ values with negligible dependence on the distance from the fault and used it to estimate the breakdown slip, $D_c$, for the 2000 $M_w$ 6.6 Tottori (0.3 m) and the 2002 $M_w$ 7.9 Denali (2.5 m) earthquakes.

The study by F&M was based on simple 2D Green's functions in a homogeneous full space for kinematic antiplane steady-state infinite-crack propagation. Thus, in their validation, F&M ignored the stress breakdown process, the free surface (FS) of the Earth, the spontaneous variability of rupture propagation, and the finiteness of the fault, and assumed that the effects of these features on $D_c''$ were negligible. Here, we numerically reexamine the methodology proposed by F&M by means of a more realistic approach, including dynamic complexity from rupture propagation on an extended fault in a half-space. Except for a kinematic source analysis used to reproduce and extend the results from F&M, we use spontaneous rupture propagation simulated by a recently developed and highly accurate approach throughout this work, namely the staggered-grid split-node (SGSN) method (Dalguer and Day, 2007) in a fourth-order staggered-grid finite difference method (Olsen, 1994). We assume a vertical strike-slip fault embedded in a homogeneous half-space (except for a test in a homogeneous full space), governed by a linear slip-weakening friction law.

## 2D Steady-State Rupture Analysis

All seismic information related to $D_c$ is contained in periods smaller than or equal to the breakdown times, $T_c$, the time required for the stress breakdown process to complete at a specific point on the fault. Thus, it is fundamental to understand whether this information is conveyed beyond the fault plane, and if so, how it varies with distance from the fault. In other words, how efficiently does this information propagate from the earthquake source to surrounding strong-motion receivers, and how detectable is it? In this section we attempt to detect and isolate the influence of wave and rupture propagation effects on the parameter $D_c''$ introduced by F&M from an infinite 2D steady-state rupture within an elastic homogeneous full space. In this simple source model, only inhomogeneous waves are excited so the ground motion is dominated by near-field terms. The fault-parallel synthetic seismograms are computed from convolution of the slip-rate functions and the Green's functions for 2D antiplane rupture models with constant rupture speed (Aki and Richards, 2002, equation 10.47).

We use the dynamically consistent slip-rate functions presented by Tinti *et al.* (2005; regularized Yoffe function) and Kostrov (1964). The regularized Yoffe function was designed to mimic slip-rate behavior consistent with dynamic rupture governed by slip-weakening friction models and is thus essentially a representation of slip rate with cohesive breakdown rupture. For instance, it has been shown that the time interval between the onset of that function and its peak value, $T_{acc}$, is proportional to the breakdown time $T_c$ (Tinti *et al.*, 2005). The Kostrov function is an analytical slip-rate function for self-similar 2D crack propagation without any cohesive mechanism during rupture. Our simulations with the Kostrov function provide a means to evaluate the method by F&M by testing whether the parameter $D_c''$ is close to zero for noncohesive rupture propagation, that is, where $D_c$ by definition is zero.

### Cohesive Rupture

Following F&M, we compute synthetic seismograms by convolving the regularized Yoffe slip-rate function (Tinti *et al.*, 2005; dashed line in Fig. 1a) with the 2D antiplane crack Green's function. Figure 1a shows a set of fault-parallel velocity and displacement seismograms computed every 400 m along a line perpendicular to the fault. In this example, we chose $T_{acc} = 0.2$ sec, a rise time of 3 sec, a total slip of 1 m, and a rupture velocity $V_R = 0.9V_S$. All traces have been shifted in time so that their velocity peaks are aligned with the origin time, defining the $D_c''$ values proposed by F&M simply as the values of the displacement at the origin, multiplied by two. In our simple rupture model only *SH*-scalar waves are generated. As a consequence, the rupture velocity

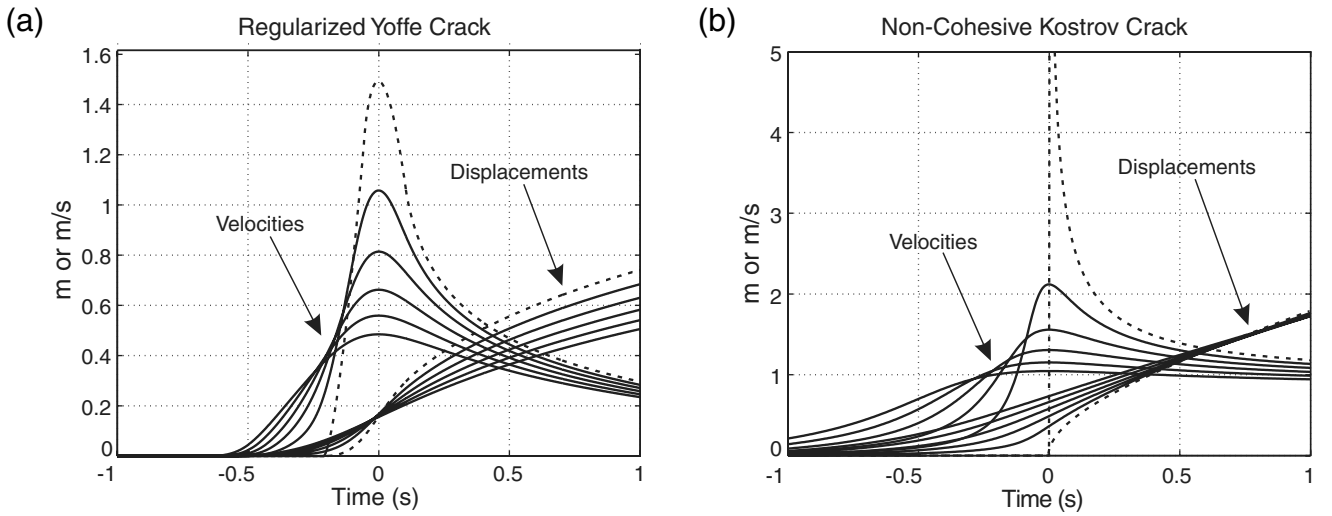


**Figure 1.** Fault-parallel displacement and velocity seismograms (aligned at the origin time with the velocity peak) computed every 400 m starting from the fault surface (source time functions in dashed lines) assuming (a) a regularized Yoffe slip-rate function (Tinti *et al.*, 2005) and (b) a singular noncohesive Kostrov slip-rate function. We have used Green's functions for a 2D antiplane infinite steady-state rupture propagating with subshear velocity.

has a strong effect on the frequency content of the synthetic seismograms. The closer $V_R$ is to $V_S$, the larger the amounts of high frequencies preserved in the synthetic seismograms independent of the distance from the source. Our results closely reproduce those presented by F&M (see their figure 1b), where $D_c''$ is consistently close to $D_c'$ with increasing distance from the fault. This result, which is valid for various rupture parameterizations (not shown), was used by F&M to justify the reliability and robustness of their method to estimate $D_c$ from $D_c''$. However, the validity of the method by F&M requires that the recorded waveforms include energy at frequencies sufficiently high to contain information about $D_c$, which was not addressed in their study.

Let us first examine the breakdown-process related-energy loss with distance from the fault in the analysis by F&M. Mikumo *et al.* (2003) and Fukuyama *et al.* (2003) have shown that, for a range of rupture conditions, the time interval between the onset of the slip-rate function and its peak value is close to the breakdown time $T_c$. Thus, let us assume that $T_c$ is given, in our 2D model, by the $T_{\text{acc}}$ parameter of the regularized Yoffe slip-rate function (Tinti *et al.*, 2005). We have computed fault-parallel velocity seismograms for different rupture cases along a fault-perpendicular line up to a distance of 3 km from the source, considering a shear-wave velocity $V_S = 3.5$ km/sec and five different values of $T_c = 0.1, 0.2, 0.4, 0.6$, and 0.8 sec. Then, we measure the spectral amplitude of the harmonics corresponding to the prescribed breakdown periods $T_c$ as a function of distance from the fault (Fig. 2a). The breakdown frequency, $f_c = 1/T_c$, thus represents a reasonable estimate of the lowest frequency containing information of $D_c$ (see also Guatteri and Spudich, 2000). Figure 2a shows the amplitude of these harmonics for the five selected breakdown frequencies. Note the expected rapid loss of energy with distance from the fault, where the higher $f_c$, the faster the loss. To examine whether the rapid energy loss with distance from the fault has implications for the method introduced by F&M, Figure 2b presents $D_c''$ values as a function of fault distance for the five rupture cases. Surprisingly, there is no correlation between the exponential attenuation shown in Figure 2a and the variation of $D_c''$ with distance from the fault: $D_c''$ remains close to $D_c'$ for fault–receiver distances at least up to 3 km. Notice that despite the similarity of $D_c''$ and $D_c'$ with increasing distance from the fault, the amplitude of the harmonic for a breakdown time $T_c = 0.4$ sec (i.e., for a breakdown frequency $f_c = 2.5$ Hz) is smaller than 10% and 1% of its original value at the source at distances of 1 and 1.5 km, respectively, from the fault. This rapid energy loss is in agreement with Dunham and Archuleta (2005), who concluded that a waveform may become irresolvable at distances beyond which its amplitude drops to about 5% of its amplitude at the source. In our selected model, this distance is only 1.2 km from the fault (see Fig. 2a).

In our previous analysis, we use the time span $T_c$ as the minimum resolvable period ($T_{\text{min}}$) associated with the breakdown process. Following Dunham and Archuleta (2005), another estimate of this period could be achieved through the minimum wavelength, approximately equal to the distance $L$ between the fault and the receiver, divided by the $S$-wave velocity ($T_{\text{min}} \approx L/V_S$). For $V_S = 3.5$ km/sec and $L = 1.4$ km this period is $T_{\text{min}} \approx 0.4$ sec ($f_{\text{max}} \approx$ 2.5 Hz), in agreement with our analysis using $T_c$. In other words, our analysis with the simple 2D cohesive model shows that off-fault displacements at peak particle velocities are insensitive to frequencies carrying information of $D_c$. Thus, the similarity between $D_c'$ and $D_c''$ in the results presented previously, which was obtained with the procedure used by F&M to validate their method, is unrelated to the

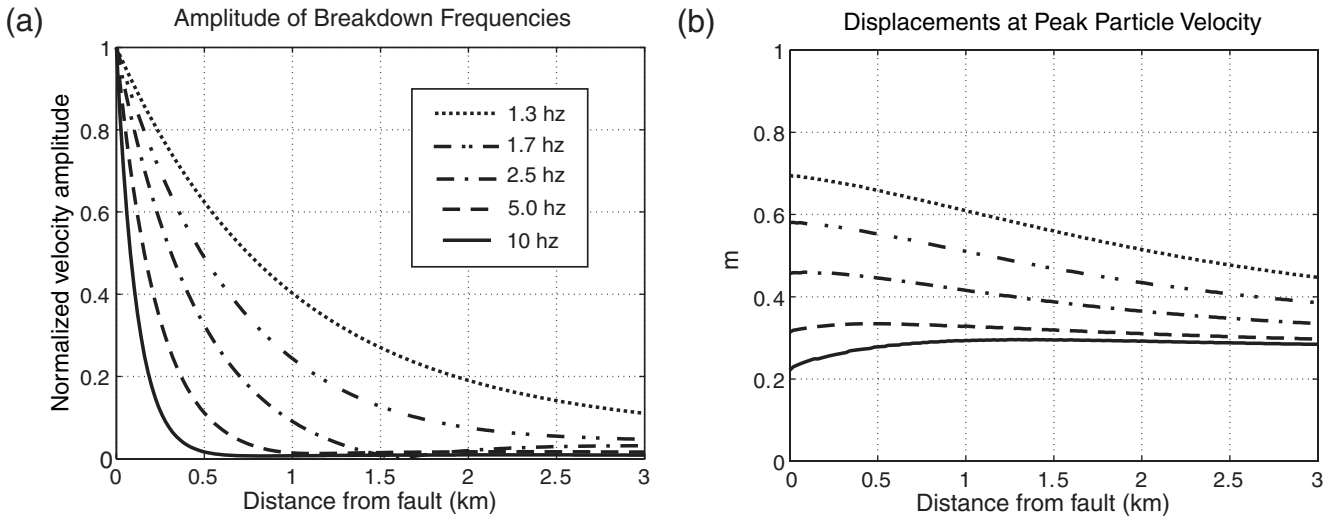


**Figure 2.** (a) Spectral particle velocity for five different breakdown frequencies of the Yoffe slip-rate functions (i.e., inverse of $T_{acc}$ parameters, listed in the inset panel) as a function of distance to the fault. (b) Fault-parallel displacements at the time of the peak particle velocities as a function of distance from the fault for the rupture scenarios listed in (a).

breakdown process. Note also that the extent of the region around the fault, inside which periods containing information of $D_c$ (i.e., periods comparable to the breakdown times $T_c$) can be resolved, is case dependent: the shorter the periods, the smaller the region. Unfortunately, because those periods are unknown *a priori* for real earthquakes, the extent of this region may always remain uncertain.

### Noncohesive Rupture

The regularized Yoffe slip-rate function used in the tests described previously is derived from dynamic cohesive rupture models. Here, we examine the performance of the F&M method for a noncohesive rupture. The breakdown process takes place instantaneously (i.e., $D_c = 0$ m), and we thus expect negligible $D_c''$ values for any distance from the fault. Causes for $D_c''$ to differ from zero include wave and rupture propagation effects, unrelated to the breakdown process.

Kostrov (1964) obtained an analytical expression for the slip-rate function of a self-similar 2D crack propagating with sub-Rayleigh rupture velocity. In this model, the slip-rate function presents a square-root singularity similar to the stress field at the crack tip. While this slip-rate function is clearly unrealistic because the breakdown frequency is infinite, it allows us to isolate and examine effects unrelated to the breakdown process that may affect the parameter $D_c''$. Following the procedure introduced in the previous section, we have computed off-fault seismograms sampled every 400 m from the fault by convolving the Green's functions with the Kostrov slip-rate function (dashed line in Fig. 1b). Here, we consider a sub-Rayleigh rupture velocity $V_R = 0.8V_S$ and the same elastic properties as before. Figure 1b reveals a strong dependence of $D_c''$ with distance from the fault. The F&M method predicts displacement values from about 0.25 m at the closest station (i.e., $D_c'' = 0.5$ m) up to about 0.7 m (i.e., $D_c'' = 1.4$ m) at a distance of 2 km from the fault. If we consider a wave speed more suitable for superficial layers (e.g., $V_S = 1.5$ km/sec) and a faster subshear rupture velocity (e.g., $V_R = 0.9V_S$), $D_c''$ values vary from about 0.8 up to 2.8 m at the same locations (not shown). In order for $D_c''$ to be a reasonable approximation of $D_c$ on the fault for noncohesive ruptures, we expect displacements at peak velocities close to zero. However, because this is not the case, our experiment confirms that $D_c''$ is dominated by wave and rupture propagation effects.

## Spontaneous Rupture Model

In the following sections, we analyze near-field strong-motion synthetics and the derived parameter $D_c''$ using realistic 3D spontaneous rupture scenarios. These scenarios are simulated with the SGSN dynamic rupture model (Dalguer and Day, 2007) using a fourth-order staggered-grid finite difference parallel code (Olsen, 1994). This method has a flat free-surface condition (Gottschaemmer and Olsen, 2001) at the top and perfectly matched layers absorbing boundaries along all other external edges of the model preventing undesired wave reflections (Marcinkovich and Olsen, 2003). Simulations presented here correspond to vertical right-lateral strike-slip faults, most of them reaching the FS of a homogeneous elastic half-space. The geometry of the problem is shown in Figure 3 and corresponds to that used in the 3D Spontaneous Rupture Code Validation Project problem version 5-9, spearheaded by the Southern California Earthquake Center (SCEC) (Harris *et al.*, 2009). The elastic properties of the medium are $V_S = 3.464$ km/sec and $V_P = 6.0$ km/sec for the $S$-wave and $P$-wave velocities, respectively, and $\rho = 2.67$ g/cm$^3$ for the density. We assume a linear slip-weakening constitutive relationship on the fault, which is a simple but well-defined friction model derived

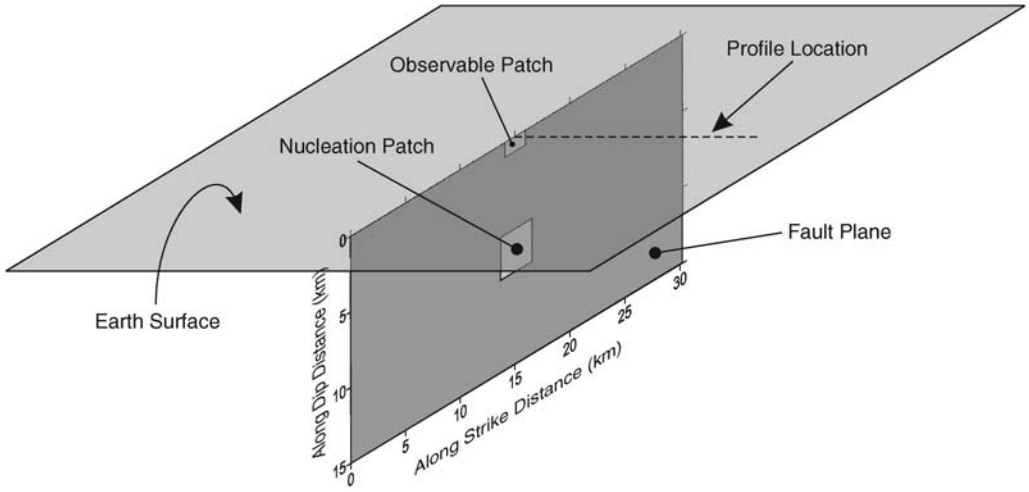


**Figure 3.** Geometry of the 3D strike-slip spontaneous rupture model used in our study. The line perpendicular to the fault depicts a profile used for display of synthetics.

from both experimental observations and theoretical considerations (Ida, 1972; Palmer and Rice, 1973; Andrews, 1976; Ohnaka and Yamashita, 1989; Matsu'ura *et al.*, 1992). This model has been used by many seismologists to study earthquakes (e.g., Day, 1982; Virieux and Madariaga, 1982; Ide and Takeo, 1997; Olsen *et al.*, 1997; Madariaga *et al.*, 1998; Oglesby *et al.*, 2000; Peyrat *et al.*, 2001; Dalguer *et al.*, 2002; Cruz-Atienza and Virieux, 2004) and has three constitutive parameters defining the friction behavior on the fault: the static ($\mu_s$) and dynamic ($\mu_d$) coefficients of friction, and the slip-weakening distance (i.e., breakdown slip), $D_c$, already discussed in previous sections. Thus, after rupture initiation, the strength of the fault in our model is given by the product of the fault normal stress, $\sigma_n$, and the friction coefficient, which decreases linearly with slip from its static value, $\tau_s = \mu_s\sigma_n$, to its dynamic level, $\tau_d = \mu_d\sigma_n$. In order to present spatially representative and robust observations from the spontaneous ruptures, our estimates of $D_c''$ presented in the following for different distances from the fault are averaged over a fault-parallel distance range of $\pm 5$ km from the epicenter. In all cases, the associated standard deviations are smaller than 3% of the average values. Simulations in the following sections were carried out on parallel supercomputers, most of them using about 1000 processors on the San Diego Supercomputer Center (SDSC) DataStar and BlueGene clusters. Wall-clock times for the simulation ranged between 1 and 1.4 hr.

### Free-Surface Amplification

In this section, we briefly summarize the effects of the FS on $D_c''$. F&M defined $D_c''$ as twice the rake-parallel free-surface displacement at the time of the peak particle velocity, where the factor of 2 arises from the hypothesis of an equal amount of opposite displacement on either side of the fault. They introduced this definition from simple models based on 2D rupture scenarios embedded in homogeneous full spaces. Here, we evaluate whether the argument used to introduce the factor of 2 is valid in a half-space. Simulations in this section were carried out with a grid size of 200 m for which rupture propagation is numerically well resolved given our model parameterization (Dalguer and Day, 2007).

Figure 4 presents velocity (dashed curves) and displacement (solid curves) synthetic seismograms computed along the dashed profile line of Figure 3, shifted in time in such a way that they are aligned with respect to the peak velocity at the origin. Velocity and displacement traces with higher amplitudes were obtained, including an FS and those with lower amplitude without an FS (i.e., within a full space). Receivers were located at distances of 0–1 km from the fault. The rupture model parameterization is shown with the label FS in Table 1. The synthetic seismograms illustrate the well-known amplification effect due to the incidence of seismic waves onto the FS. Both velocities and displacements are much smaller in the absence of the FS, independent of the distance from the fault. The corresponding effect on $D_c''$ is shown in Figure 5, where we present average rake-parallel displacements at the time of the peak velocities for models with and without FS as a function of distance perpendicular to the fault. Figure 6 shows a map of the ratio between these displacement values obtained with and without the FS. Both figures show that $D_c''$ is affected by an amplification factor of around two within the area of analysis due to the FS. The small areas with amplification factors of 3 or larger are due to differences in later energetic arrivals generated at the fault edges that could not be discriminated automatically by our algorithm.

In summary, our results suggest that the method by F&M would overestimate $D_c$ by a factor of 2 due to the correction to account for the equal amount of opposite displacements on either side of the fault. Given that the FS already induces an amplification of the same order, the definition of $D_c''$ that we will use in the following does not adopt the correction factor of 2 considered by F&M.

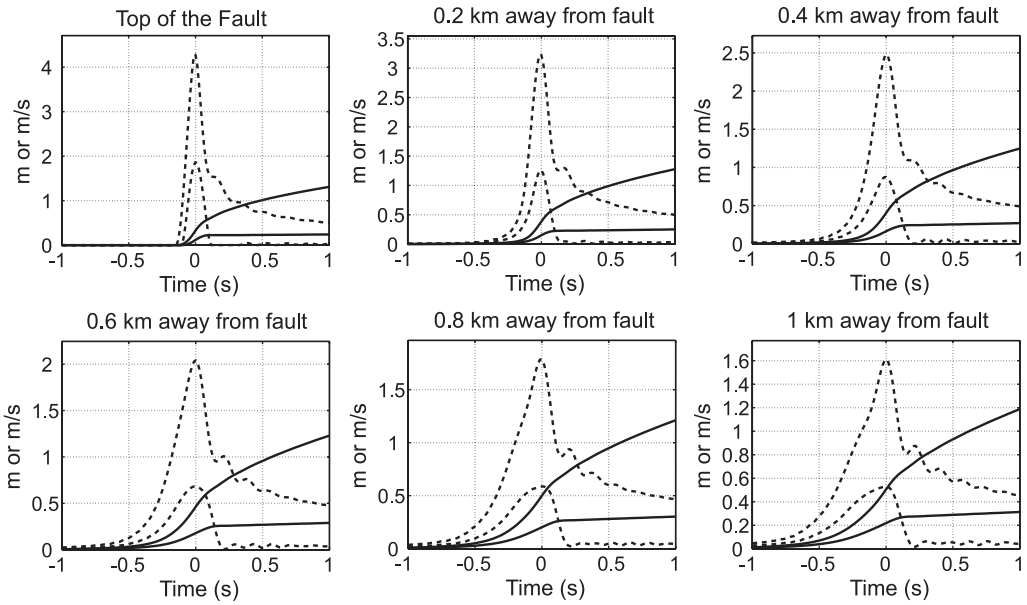


**Figure 4.** Strike-parallel displacement (solid curve) and velocity (dashed curve) seismograms computed along the profile shown in Figure 3 with (higher amplitudes) and without (lower amplitudes) an FS.

### $D_c''$ from Spontaneous Rupture Models with Surface Rupture

In this section, we examine whether the parameter $D_c''$ represents a reliable estimate of $D_c$ using near-fault synthetic seismograms from realistic 3D spontaneous rupture scenarios. These scenarios are simulated with the 3D medium described previously and a set of dynamic rupture models that break the FS with various combinations of breakdown slip ($D_c$), dynamic stress drop ($\Delta\tau = \tau_0 - \tau_d$, where $\tau_0$ is the initial shear stress), and fracture energy ($G_c$). To determine whether each of those fundamental parameters has a characteristic effect on $D_c''$ or not, three model sets of frictional and initial conditions parameterization are considered: A, B, and C. Case A considers four models for which the breakdown strength drop ($\tau_s - \tau_d$) remains the same, but $D_c$, $\Delta\tau$, and $G_c$ vary. The values of these parameters increase from model A1 to A4, as shown in Figure 7a. Case B considers four models in which $D_c$ varies with each model, as in case A, but where $\Delta\tau$ and $G_c$ remain the same for all the four models. Note that $\tau_s$ decreases with increments of $D_c$, as shown in Figure 7b, in order for the rupture to propagate across the entire fault. Case C considers three models in which $\Delta\tau$ varies but $D_c$ and $G_c$

Table 1

3D Spontaneous Rupture Model Parameters Used in This Work

| | Outside Nucleation | | | | | | Inside Nucleation | | | | |
|---|---|---|---|---|---|---|---|---|---|---|---|
| Model Name | $\tau_0$ (MPa) | $\sigma_0$(MPa) | $\mu_s$ | $\mu_d$ | $D_c$ (m) | $\Delta\tau$ (MPa) | $\tau_0$ (MPa) | $\sigma_0$(MPa) | $\mu_s$ | $\mu_d$ | $D_c$ (m) |
| FS | 70.0 | 120.0 | 0.677 | 0.525 | 0.4 | 7.0 | 81.6 | 120.0 | 0.677 | 0.525 | 0.4 |
| A1 | 70.0 | 120.0 | 0.677 | 0.525 | 0.4 | 7.0 | 81.6 | 120.0 | 0.677 | 0.525 | 0.4 |
| A2 | 72.0 | 120.0 | 0.677 | 0.525 | 0.6 | 9.0 | 81.96 | 120.0 | 0.677 | 0.525 | 0.6 |
| A3 | 74.0 | 120.0 | 0.677 | 0.525 | 0.8 | 11.0 | 81.96 | 120.0 | 0.677 | 0.525 | 0.8 |
| A4 | 76.0 | 120.0 | 0.677 | 0.525 | 1.0 | 13.0 | 81.96 | 120.0 | 0.677 | 0.525 | 0.4 |
| B1 | 70.0 | 120.0 | 0.692 | 0.525 | 0.4 | 7.0 | 83.87 | 120.0 | 0.692 | 0.525 | 0.4 |
| B2 | 70.0 | 120.0 | 0.636 | 0.525 | 0.6 | 7.0 | 83.87 | 120.0 | 0.692 | 0.525 | 0.6 |
| B3 | 70.0 | 120.0 | 0.608 | 0.525 | 0.8 | 7.0 | 83.87 | 120.0 | 0.692 | 0.525 | 0.8 |
| B4 | 70.0 | 120.0 | 0.592 | 0.525 | 1.0 | 7.0 | 77.81 | 120.0 | 0.642 | 0.525 | 1.0 |
| C1 | 140.0 | 240.0 | 0.677 | 0.525 | 0.8 | 14.0 | 163.2 | 240.0 | 0.677 | 0.525 | 0.8 |
| C2 | 143.0 | 240.0 | 0.677 | 0.525 | 0.8 | 17.0 | 163.2 | 240.0 | 0.677 | 0.525 | 0.8 |
| C3 | 146.0 | 240.0 | 0.677 | 0.525 | 0.8 | 20.0 | 163.2 | 240.0 | 0.677 | 0.525 | 0.8 |

$\tau_0$ is the initial fault shear stress; $\sigma_0$ is the initial fault normal stress; $\mu_s$ and $\mu_d$ are the static and dynamic friction coefficients, respectively; $D_c$ is the breakdown slip (i.e., the slip-weakening distance); and $\Delta\tau$ is the dynamic stress drop. The model with label FS is used in the Free-Surface Amplification section; models with labels A1, A2, A3, and A4 are used in the Case A: Variable $D_c$, Stress Drop, and Fracture Energy section; models with labels B1, B2, B3, and B4 are used in the Case B: Constant Stress Drop and Fracture Energy, Variable $D_c$ section; and models with labels C1, C2, and C3 are used in both the Case C: Constant Breakdown Slip and Fracture Energy, Variable Stress Drop section and the Estimates of the Resolution Distance for $D_c$ ($R_c$) section.

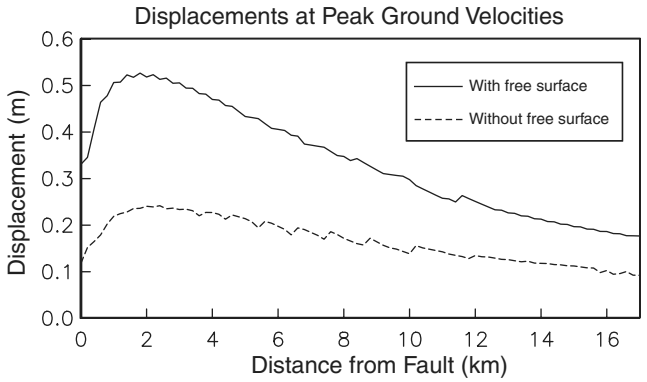


**Figure 5.** Values of strike-parallel displacements at the time of the peak velocities along the profile shown in Figure 3 with and without an FS.

remain constant, as shown in Figure 7c. The three sets of models are parameterized to ensure that the rupture propagates with subshear speed throughout the fault.

*Case A: Variable $D_c$, Stress Drop, and Fracture Energy.* The four case-A models are shown in Figure 7a and summarized in Table 1 (with labels A1, A2, A3, and A4). Figure 8 shows velocity and displacement seismograms at various distances from the fault along the dashed profile line shown in Figure 3. The grid resolution of these simulations is 200 m, and the seismograms are shifted in time so that the peak velocities are aligned with the origin. The results suggest that the greater $D_c$ on the fault, the higher the displacements and velocities at the origin time for any distance. In other words, there appears to be a direct correlation between $D_c$ and $D_c''$. This finding is further illustrated in Figure 9, where we show average estimates of $D_c''$ for each rupture case as a function of distance from the fault. Contrary to the results reported by F&M, which are similar to those shown in Figure 2b, Figure 9 depicts a strong near-fault variation of $D_c''$. This variation includes a minimum on top of the fault and increasing values

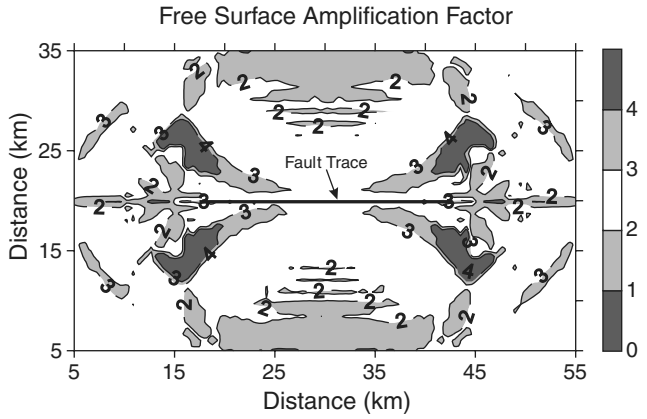


**Figure 6.** Ratio between the strike-parallel displacements at the time of the peak velocities, computed with and without an FS (i.e., free-surface amplification factor map).

up to a maximum around 2 km from the fault. Then, at further distances, a slow asymptotic decrease appears with distance. These results suggest that $D_c$ and $D_c''$ are correlated, even at distances of several kilometers from the fault.

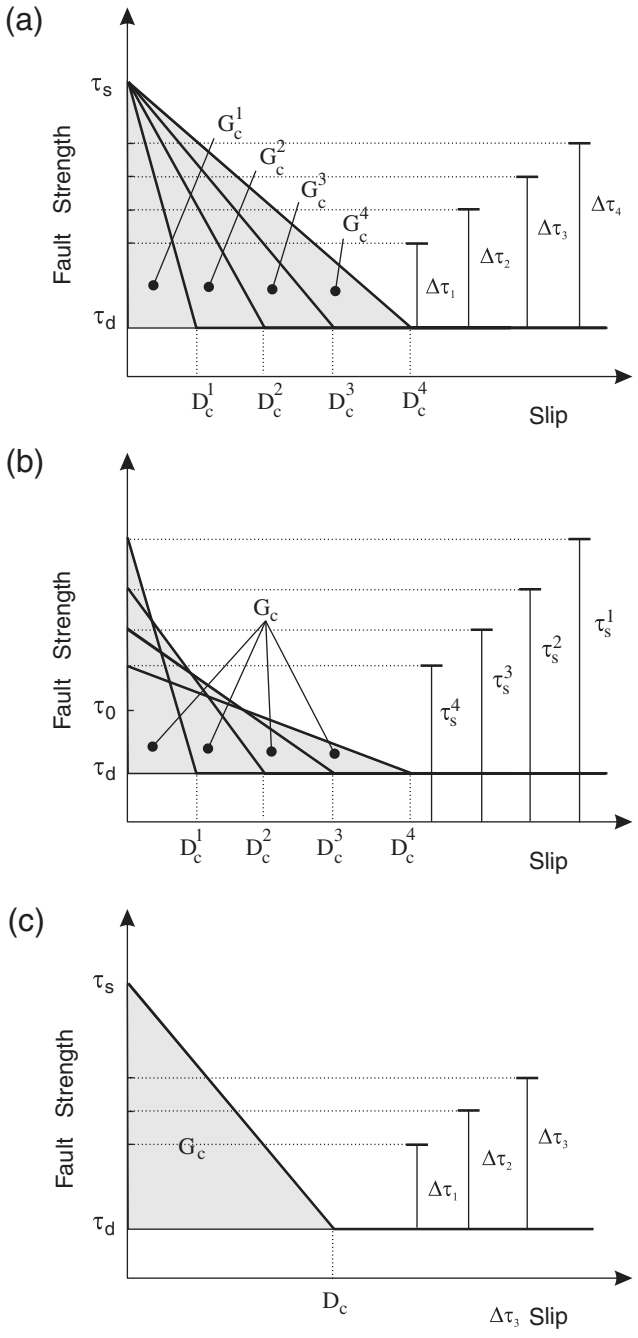


**Figure 7.** Slip-weakening friction models used in our 3D spontaneous rupture tests of (a) the Case A: Variable $D_c$, Stress Drop, and Fracture Energy section (see Table 1, models A1, A2, A3, and A4 with constant breakdown strength drop, $\tau_s - \tau_d$); (b) the Case B: Constant Stress Drop and Fracture Energy, Variable $D_c$ section (see Table 1, models B1, B2, B3, and B4 with constant dynamic stress drop, $\Delta\tau$, and fracture energy, $G_c$); and (c) the Case C: Constant Breakdown Slip and Fracture Energy, Variable Stress Drop section (see Table 1, models C1, C2, and C3 with constant breakdown slip, $D_c$, and fracture energy, $G_c$).

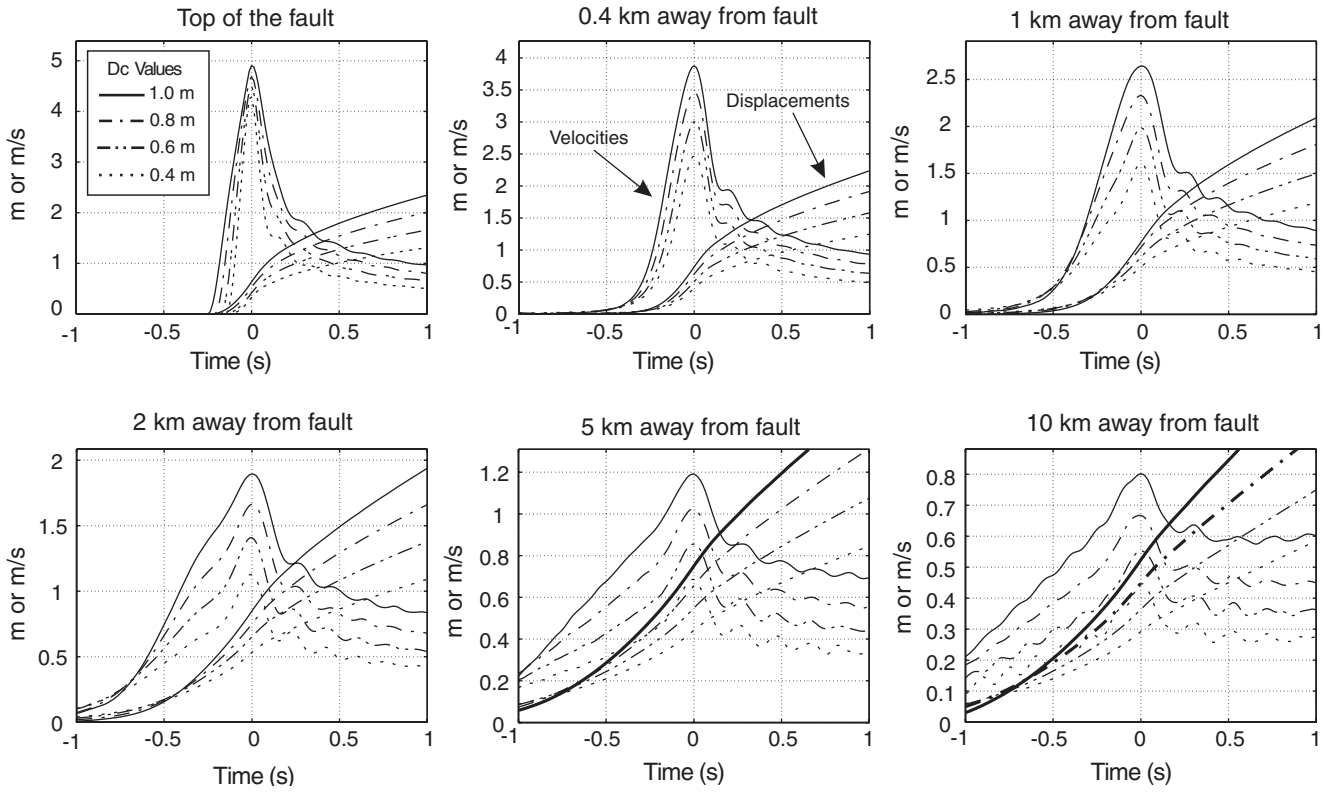


**Figure 8.** Strike-parallel displacement and velocity seismograms (aligned at the origin time with the first velocity peak) computed along the profile shown in Figure 3 for the four slip-weakening friction models illustrated in Figure 7a, with parameters given in Table 1 for models A1, A2, A3, and A4.

However, in these simulations not only the breakdown slip $D_c$ has changed between the rupture scenarios but also the dynamic stress drop $\Delta\tau$ and the fracture energy $G_c$. For this reason, differences among $D_c''$ along the profiles cannot be attributed to the variation of $D_c$ alone, and additional tests are needed.

*Case B: Constant Stress Drop and Fracture Energy, Variable $D_c$.* Let us consider four additional rupture scenarios, those of case B with constant stress drop and fracture energy but variable breakdown slip (Fig. 7b, Table 1 with labels B1, B2, B3, and B4). The spatial grid step is decreased to 50 m for these simulations in order to resolve $D_c''$ sufficiently close to the fault. Velocity and displacement seismograms are shown in Figure 10 for all rupture scenarios, and average $D_c''$ values computed with distance from the fault are shown in Figure 11. Notice that the variation of $D_c''$ is largest within a few hundred meters of the fault (depending on the rupture scenario) and decreasing at larger distances from the fault. The inner region of a few hundred meters width, not clearly present in the case-A results, is characterized by a rapid attenuation of velocity amplitudes with distance from the fault. Outside this region, $D_c''$ has essentially the same value for all rupture scenarios. These results suggest that $D_c''$ may only be sufficiently sensitive to $D_c$ within a short distance from the fault and that it is controlled by the variation in dynamic stress drop and/or fracture energy beyond this distance.

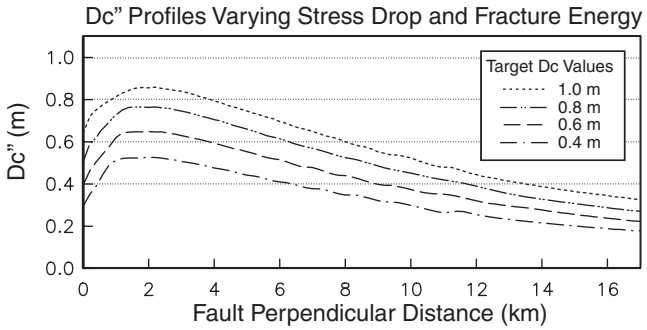


**Figure 9.** Average $D_c''$ values as a function of distance to the fault (see text). Each curve corresponds to a single slip-weakening friction model from Figure 7a with parameters listed in Table 1 for models A1, A2, A3, and A4. Horizontal lines depict the prescribed $D_c$ values on the fault.

*Case C: Constant Breakdown Slip and Fracture Energy, Variable Stress Drop.* In the case-C experiments, both the slip-weakening distance, $D_c$, and the fracture energy, $G_c$, are constant, and the only parameter variable among the scenarios is the dynamic stress-drop, $\Delta\tau$ (see Fig. 7c and Table 1, models C1–C3). Figure 12 presents the average $D_c''$ profiles as a function of distance from the fault. The results show that outside a very narrow region next to the fault with a width of about 300 m (see inset of Fig. 12), where $D_c''$ estimates

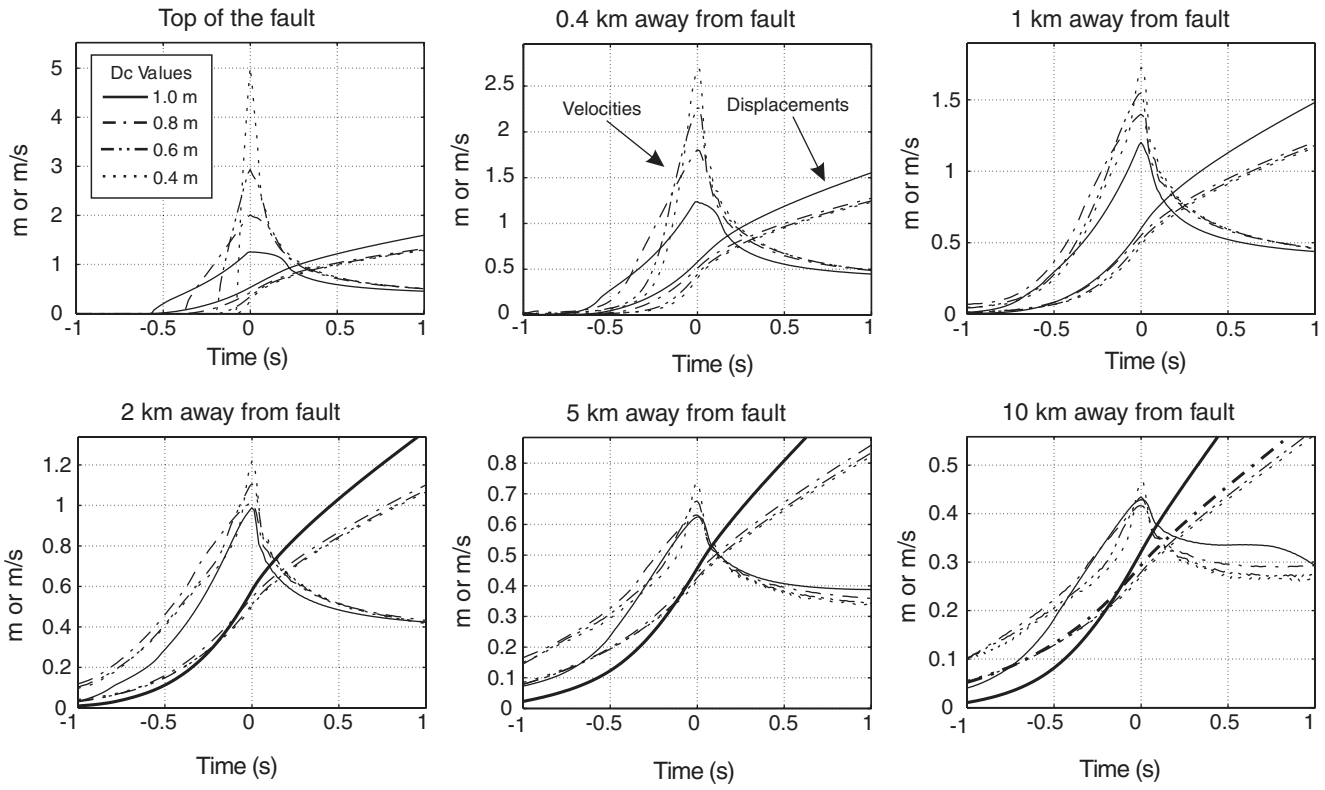


**Figure 10.** Strike-parallel displacement and velocity seismograms (aligned at the origin time with the first velocity peak) computed along the profile shown in Figure 3 for the four slip-weakening friction models illustrated in Figure 7b, with parameters given in Table 1 for models B1, B2, B3, and B4.

remain close to each other for all rupture scenarios, $D_c''$ is proportional to $\Delta\tau$, similar to the case-A models (see Fig. 9) for which $\Delta\tau$ also varies. Thus, beyond this narrow zone, $D_c''$ appears to be highly sensitive to the variation of $\Delta\tau$ rather than $D_c$ or $G_c$, at least for ruptures that break the surface.

In summary, our sequence of spontaneous rupture experiments A, B, and C with surface rupture indicate that, except for a very narrow zone next to the fault (approximately 300 m length in our last experiment) where $D_c''$ varies less than about 25%, $D_c''$ is only affected by the dynamic stress drop of the earthquake.

### $D_c''$ from Buried Fault Models and the 2004 Parkfield Earthquake

So far, all 3D rupture tests we have conducted assumed that the rupture reached the surface of the Earth. Now, let us examine $D_c''$ estimated from spontaneous ruptures that stop

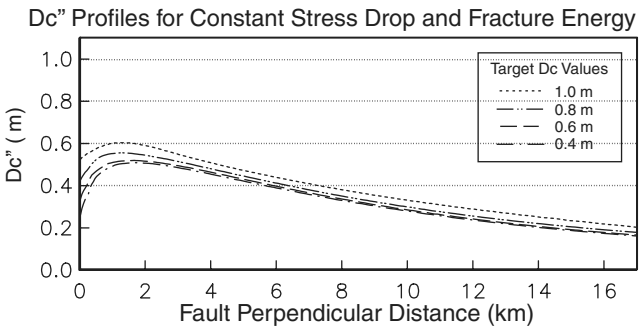


**Figure 11.** Average $D_c''$ values as a function of distance to the fault. Each curve corresponds to one slip-weakening friction model of Figure 7b, with parameters given in Table 1 for models B1, B2, B3, and B4. The horizontal lines depict the prescribed $D_c$ values on the fault.

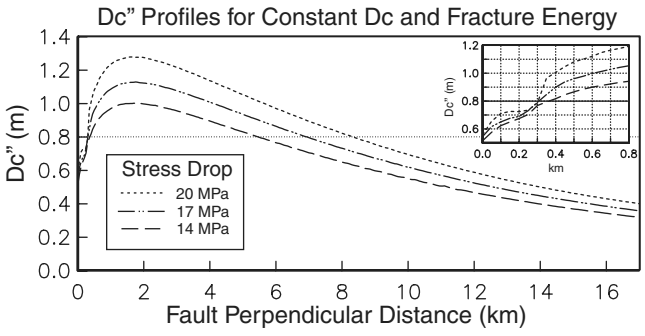


**Figure 12.** Average $D_c''$ values as a function of distance to the fault. Each curve corresponds to individual slip-weakening friction models of Figure 7c, with parameters given in Table 1 for models C1, C2, and C3. The horizontal lines depict the prescribed $D_c$ value on the fault equal to 0.8 m.

short of breaking the ground surface. For that purpose we use model B2 with $D_c = 0.6$ m (see Table 1 and Fig. 7b) in two scenarios, with the top of the fault buried (1) 250 m and (2) 500 m below the FS. Figure 13 shows the average $D_c''$ along profiles at the Earth's surface as a function of distance perpendicular to the fault projection on the Earth's surface. The $D_c''$ values are dramatically different from the $D_c$ target value at all distances from the fault, with larger discrepancies for larger depth of burial of the fault. In fact, $D_c''$ tends to zero, independent of the source depth as we get closer to the surface fault projection. This result implies that rake-parallel displacements tend to disappear along the surface projection of the fault, which acts as a nodal region for $D_c''$. In summary, this test shows that, as obtained for scenarios with surface ruptures beyond a narrow region next to the fault, $D_c''$ does not carry measurable information about $D_c$ at any distance from the fault projection when rupture does not reach the Earth's surface.

The $M_w$ 6.0 2004 Parkfield earthquake probably represents the earthquake with the highest amount of near-fault observations ever recorded. With its right-lateral strike-slip mechanism, the rupture propagated with subshear velocity from southeast to northwest (Liu *et al.*, 2006; Ma *et al.*, 2008). Geologic mapping has revealed no coseismic surface rupture (Rymer *et al.*, 2006), but high-resolution kinematic-rupture waveform inversions by Liu *et al.* (2006) show that rupture may have propagated to within about 1 km of the surface, near the northwestern edge of the fault, about 20 km from the hypocenter. Figure 14 shows most of the seismic stations that recorded strong-motion seismic data from this event within a radius of 35 km. We have selected five of the closest stations (enclosed by rectangles in Fig. 14), all within 1.5 km of the fault trace, with some of them (e.g., GH1W and FZ15) less than 200 m from the fault surface projection. Figure 15a shows the first 20 sec of the unfiltered fault-parallel velocities.

Ma *et al.* (2008) have proposed dynamic rupture models for the 2004 Parkfield earthquake. Their preferred model (B) explains observed seismograms in the frequency range between 0.16 and 1.0 Hz reasonable well and assumes a

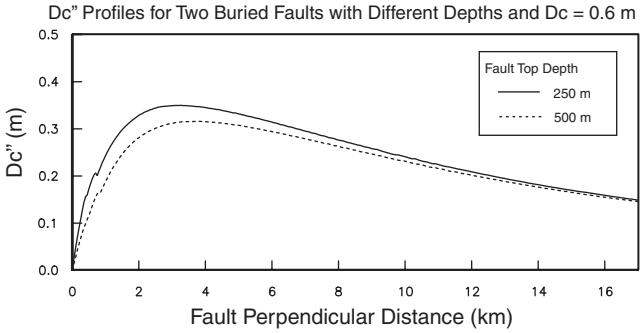


**Figure 13.** Average $D_c''$ values as a function of distance to the fault. Each curve corresponds to the slip-weakening friction model labeled B2 in Table 1 but with different fault depths as described within the inset panel.

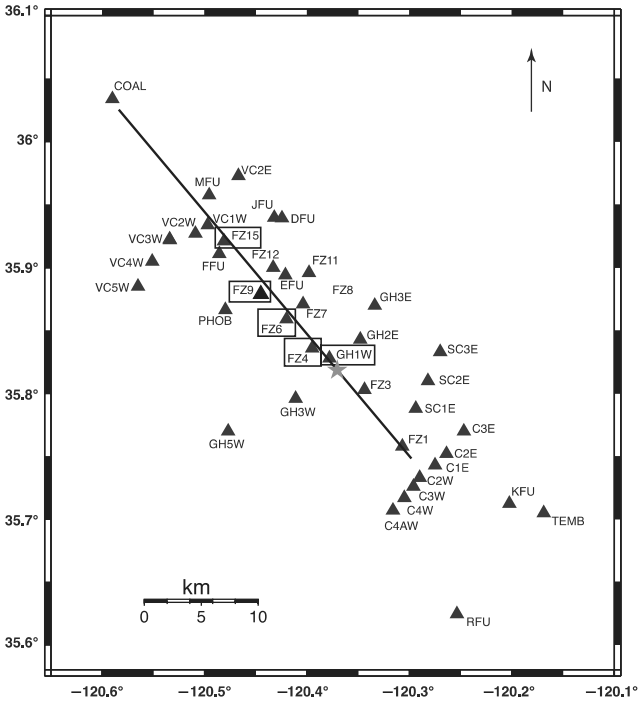


**Figure 14.** Most of the seismic stations (black triangles) deployed around the trace of the causative fault for the 2004 $M_w$ 6.0 Parkfield earthquake (after Ma *et al.*, 2008). The gray star depicts the epicenter. Stations used in our analysis of the $D_c''$ from Buried Fault Models and the 2004 Parkfield Earthquake section are enclosed by rectangles.

constant breakdown slip of 0.15 m. Our Figure 15b shows a 2-sec time window of rake-parallel velocity and displacement seismograms aligned at the origin time with the first velocity peak. The signals are high-pass filtered with a corner frequency of 0.05 Hz to eliminate interference of low-frequency noise in the seismograms with the breakdown periods, estimated to be smaller than 0.5 sec or so after Ma *et al.* (2008) (i.e., $f_c \geq 2$ Hz). $D_c''$ estimates at all stations are found to be smaller than 0.02 m. These are negligible values for $D_c$ compared with that determined by Ma *et al.* (2008) (i.e., 10% or smaller). This result agrees with our numerical tests for buried faults, that is, the near-fault ground-motion records of the 2004 Parkfield earthquake does not contain any relevant information about $D_c$ due to the lack of coseismic surface rupture.

## Estimates of the Resolution Distance for $D_c$ ($R_c$)

Given the fast decay of high-frequency energy with distance from the fault demonstrated in our simulations, we expect the near-fault strong-motion seismic data to contain information about breakdown frequencies excited only very locally, within a very short distance from the stations. For example, the inset on Figure 12 obtained from our case-C simulations reveals that $D_c''$ suffers an abrupt change of pattern with distance at an offset from the fault of about 300 m. For distances from the fault smaller than about 300 m, $D_c''$

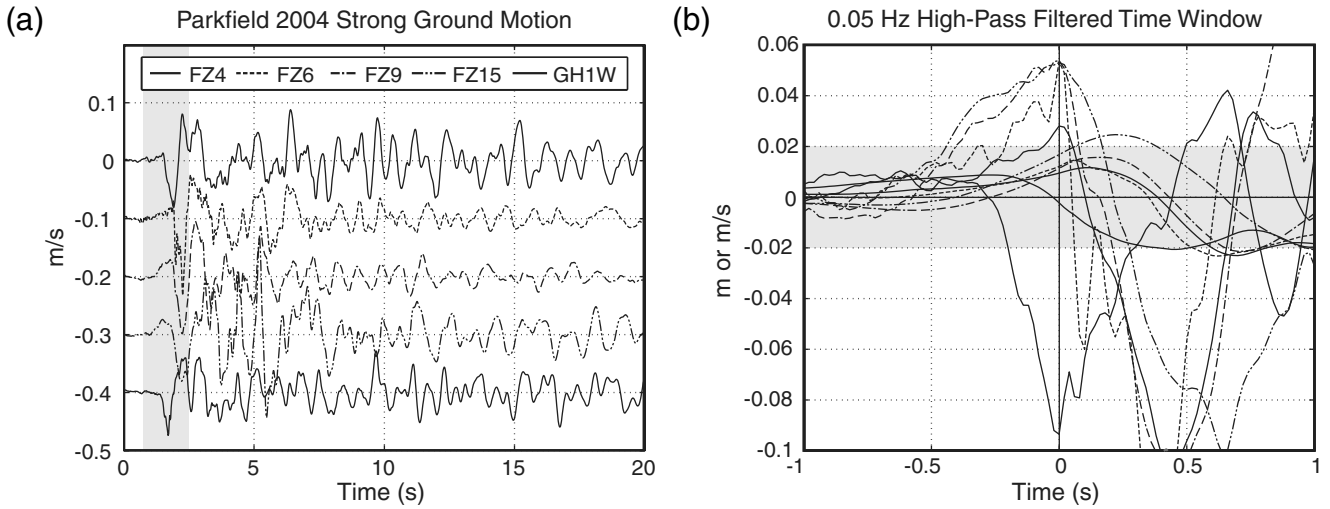


**Figure 15.** (a) Fault-parallel horizontal velocity seismograms recorded at stations enclosed by rectangles in Figure 14; (b) time windows (gray band in [a]) of high-pass filtered displacement with a cutoff of 0.05 Hz (signals with amplitude bounded by the gray band at the origin time) and velocity seismograms aligned at the origin time with the first velocity peak. The gray band depicts the region where the absolute displacement values are smaller than 2 cm.

values for all rupture scenarios remain reasonably close to each other, ranging from about 0.55 m on the fault to about 0.8 m (the target slip-weakening distance $D_c$) at 300 m from the fault. For distances from the fault larger than about 300 m, the values of $D_c''$ diverge fast and follow the general pattern determined by the dynamic stress drop $\Delta\tau$. In the following, we will refer to this distance as the resolution distance for $D_c$ or $R_c$ and to the region next to the fault bounded by this distance as the resolution zone for $D_c$. Within the resolution zone, $D_c''$ is a reasonably good estimate of $D_c$. Thus, we obtain an approximate value of $R_c$ of about 300 m for the scenarios considered in our case-C experiment. However, Figure 2a shows that this distance is case dependent because the decay rate of the energy containing information of $D_c$ depends on the frequency content of the breakdown process, which may differ from one earthquake to another. In the following, we attempt to estimate $R_c$ using two different features associated with the breakdown process.

### Estimating $R_c$ from $f_c$

The first approach to estimate $R_c$ comes directly from the attenuation law of the frequencies associated with the breakdown process. Recall that the breakdown frequency, $f_c$, is defined as the reciprocal of the breakdown period, $T_c$, measured at a point on the fault as the time between the rupture nucleation and the time at which the dynamic stress level is reached. Because of the rapid loss of energy with distance from the fault, we expect seismic waves containing breakdown frequencies recorded at a given station to be excited over a small fault patch closest to the station, with dimensions comparable to $R_c$. For example, in rupture scenarios C1–C3, the dimensions of the patch are on the order of hundreds of meters. In the following, for stations located along the profile in Figure 3, we assume a rectangular patch containing fault points from the Earth's surface to 1 km depth and 2 km horizontally, as shown in Figure 3 as the observable patch. Figure 16 shows the normalized Fourier spectral velocity at the breakdown frequency averaged over the observable patch (second column of Table 2) as a function of distance from the fault for models C1–C3. Spectral velocity amplitudes of these frequencies are 0.12–0.182 m/sec at the source, 0.02–0.045 m/sec 100 m from the fault, and 0.013–0.024 m/sec at the limit of the resolution zone (i.e., about 300 m from the fault). These values and Figure 16 show that

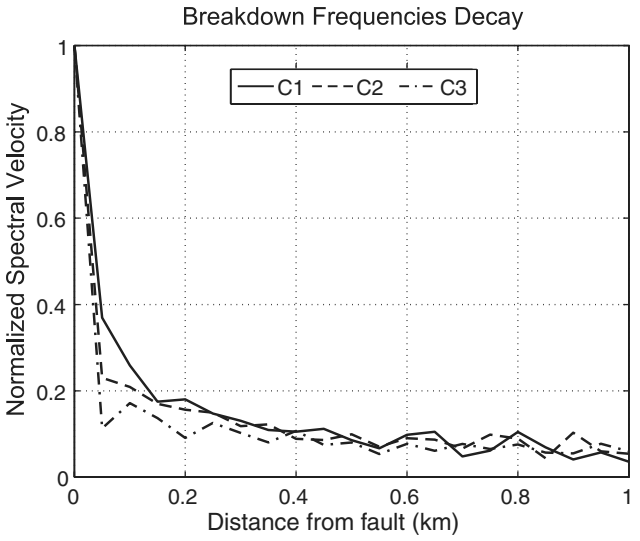


**Figure 16.** Fault-parallel spectral velocity as a function of distance from the fault along the profile shown in Figure 3 for the three slip-weakening friction models illustrated in Figure 4c (see Table 1, models C1–C3). See Table 2 for the corresponding breakdown frequencies.

Table 2
Average Values with Their Standard Deviation for the Three Rupture Scenarios C1, C2, and C3

| Rupture Model | Breakdown Frequency (Hz) | Mean Wavelength $\lambda_c$ (m) | Cohesive Zone Length $\Lambda_c$ (m) | $R_c$ from $f_c$ (m) |
|---|---|---|---|---|
| C1 ($\Delta\tau = 14$ MPa) | $7.3 \pm 1.4$ | $475 \pm 76$ | $359 \pm 19$ | $380 \pm 61$ |
| C2 ($\Delta\tau = 17$ MPa) | $9.9 \pm 1.5$ | $350 \pm 46$ | $276 \pm 22$ | $280 \pm 37$ |
| C3 ($\Delta\tau = 20$ MPa) | $12.5 \pm 1.7$ | $277 \pm 33$ | $217 \pm 21$ | $221 \pm 27$ |

the energy of the breakdown frequencies $f_c$ in all cases have been decreased by about 80% and 90% at distances of 100 and 300 m from the fault, respectively. For offsets equal to or larger than 600 m, the Fourier velocity spectral amplitudes for all scenarios are almost indistinguishable (not shown). Thus, as concluded earlier, the breakdown-process related seismic energy does not provide observable information about $D_c$ for distances larger than about 300 m.

On the other hand, the mean wavelength corresponding to the breakdown frequencies, $\lambda_c = V_S/f_c$, varies between 277 and 475 m for models C1–C3 and is listed in the third column of Table 2. From the previous analysis, we have concluded that information related to the breakdown process becomes negligible at the limit of the resolution zone (i.e., at distances of $R_c$ from the fault), that is, where the amplitudes of the breakdown frequencies decrease to about 10% of their value on the fault. Following Dunham and Archuleta (2004), under steady-state rupture conditions, the amplitude of the excited shear-wave field should then satisfy the condition $e^{-2\pi\alpha R_c/\lambda_c} = 0.1$ at a distance of $R_c$ from the fault, where $\alpha = \sqrt{1 - V_R^2/V_S^2}$. Assuming a rupture velocity $V_R = 0.9V_S$ with $V_S = 3.464$ km/sec, we find that $R_c \approx 0.8\lambda_c$. Thus, we can expect significant information about $D_c$ up to a maximum distance from the fault of about 0.8 times the mean wavelength, $\lambda_c$, corresponding to the breakdown frequency, $f_c$. The last column of Table 2 lists estimates of $R_c$ for models C1–C3 using this approach, which represents an approximation of the resolution distance for $D_c$ based on our knowledge of the mean breakdown frequency, referred to as the $f_c$ resolution distance for $D_c$.

### Estimating $R_c$ from the Cohesive Zone Length

Another spatially related measure of the breakdown period is the length of the cohesive zone, $\Lambda_c$, the width of the fault region over which the breakdown process occurs. This length corresponds to the size of the cohesive zone measured along the direction of rupture propagation. We can therefore use the distance from the rupture front to the closest points at which the shear stress has reached the dynamic friction level as an approximation of $\Lambda_c$ (e.g., Cruz-Atienza *et al.*, 2007). We have estimated $\Lambda_c$ for the C1–C3 models over the observable patch, producing average values (fourth column of Table 2) very similar to those of the $f_c$ resolution distance for $D_c$ (last column of Table 2) (i.e., $R_c \approx \Lambda_c$). Thus, we conclude that the length of the cohesive zone $\Lambda_c$ also represents a reasonable alternative to estimate $R_c$, which is the maximum distance from the fault where the breakdown process may be resolved using strong-motion seismic data. Note that (see Table 2) the bigger the stress drop of the rupture scenario, the shorter the cohesive zone (in agreement with Andrews, 2005; Day *et al.*, 2005), the higher the breakdown frequencies (in agreement with Guatteri and Spudich, 2000), and the smaller the $f_c$ resolution zone for $D_c$ (in agreement with Dunham and Archuleta, 2005).

### $R_c$ for a Stochastic Source Model

The amount of seismic radiation from an earthquake into the far field depends on the complexity of the source history. In particular, changes in rupture velocity and fault slip heterogeneities are responsible for high-frequency generation and wave propagation far from the source. Our results presented so far are derived for steady-state or spontaneous rupture conditions with rather smooth initial conditions. In this section we analyze the radiated wave field from a source model where the amount of far-field radiation is expected to be more realistic due to added complexity in rupture propagation. In particular, we use a dynamic source model that integrates a stochastically generated heterogeneous fault distribution of both strength excess ($\tau_s - \tau_0$) and dynamic stress drop ($\Delta\tau = \tau_0 - \tau_d$). This source model is obtained using a procedure similar to that introduced by Dalguer *et al.* (2008) and applied by Olsen *et al.* (2009) and Roten *et al.* (2009) to generate realistic spontaneous rupture scenarios and ground-motion estimates for southern California and Utah, respectively. The stochastic slip realization involves a von Karman autocorrelation function (Mai and Beroza, 2002) with a Hurst exponent of 1.2 and correlation lengths equal to 9 km along strike and 6 km downdip. We assumed constant values of both the fault normal stress and the breakdown slip, $D_c$ (0.4 m), and the medium properties were the same as those used in previous sections.

Figure 17 illustrates the stochastic fault rupture. The distributions of final slip and rupture velocity are heterogeneous, with acceleration and deceleration of the rupture front in several fault regions. Note that the rupture speed remains subshear throughout the fault. Breakdown frequency values ($f_c$) on the fault are highly heterogeneous and range from about 0.5 up to 5 Hz (not shown). We have computed average values of $f_c$ within five observable patches of the same size as that indicated in Figure 3. We estimate values of $f_c$ and their standard deviation at these patches, centered at distances of 5, 10, 15, 20, and 25 km from the fault edge along strike, of $2.64 \pm 0.6$, $2.44 \pm 0.5$, $1.68 \pm 0.5$, $1.60 \pm 0.3$, and $1.77 \pm 0.3$ Hz, respectively. Note that these values

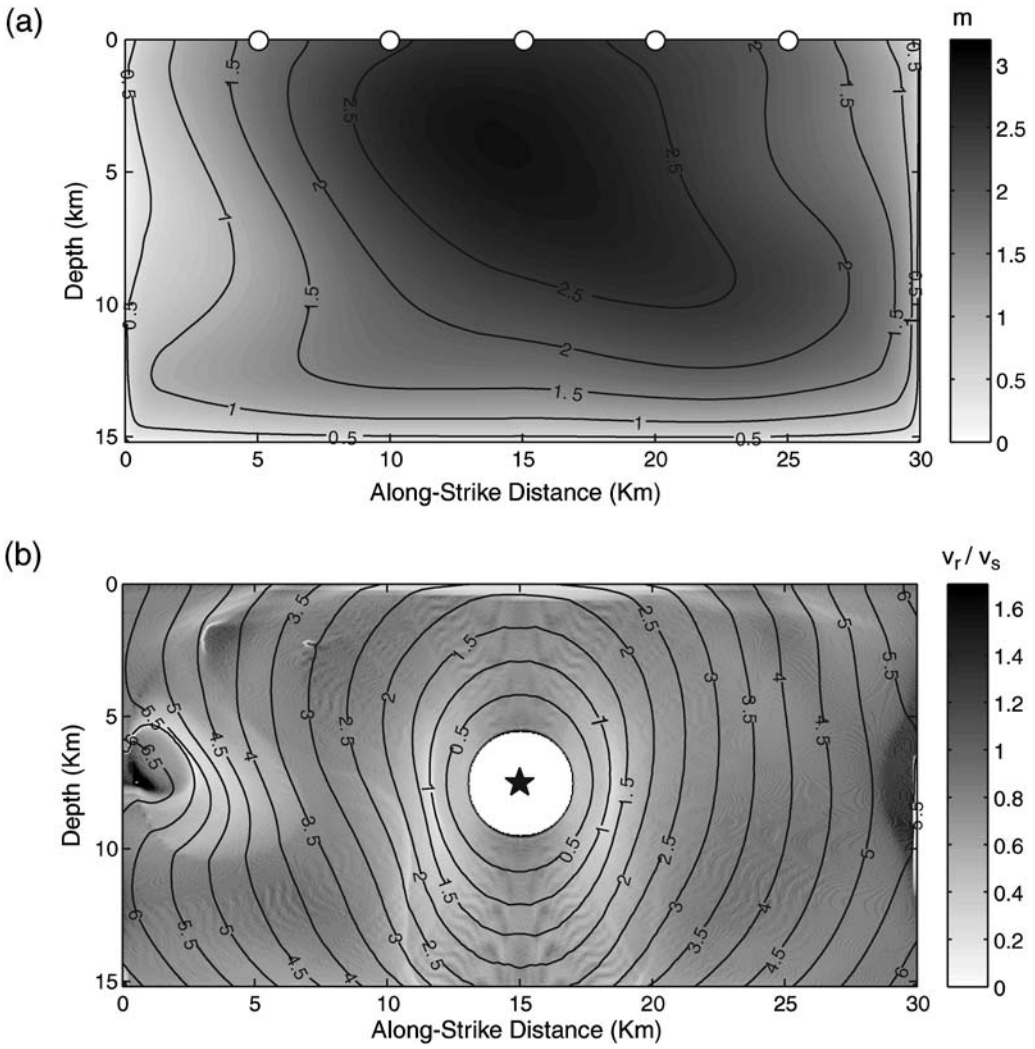


**Figure 17.** Subshear stochastic source model: (a) final slip distribution on the fault and location of the five fault-perpendicular profiles used for $D_c$ analysis (white circles) and (b) rupture-time contours (with labels in seconds) and ratios of the rupture front velocity ($V_R$) and the $S$-wave velocity ($V_S$) (gray scale map).

are 3–6 times lower than those obtained from the smooth fault results (see Table 2). The average spectral velocity decay was then estimated as a function of distance from the fault for those frequencies along five fault-perpendicular profiles centered at each observable patch (Fig. 18). Because of the lower breakdown frequencies, the spectral energy decays more slowly with distance from the fault, as compared to that for the smoother ruptures (see Fig. 16). Nevertheless, at a distance of 500 m from the fault, the seismic energy carrying information of $D_c$ has been attenuated by more than 80%. A few hundred meters further away, at a distance of 1.2 km, the energy attenuation reaches 90% indicating thus $R_c$, the resolution distance for $D_c$. Alternatively, we estimate $R_c$ from the average value of the cohesive zone width within the five observable patches to be $1.46 \pm 0.31$ km and from $f_c$ (80% of the wavelength associated with the mean $f_c$ value of 2.0 Hz) as $1.37 \pm 0.23$ km, confirming that these estimates are also reliable for a stochastic source model. Although larger than the values of $R_c$ obtained from the smooth ruptures, our results for the heterogeneous source model are consistent and indicate that $D_c$ may only be resolved within a narrow zone around the fault.

## Discussion and Conclusions

We have used several simulation approaches to test whether the parameter $D_c''$ computed using the method by F&M is capable of producing reliable estimates of the breakdown slip $D_c$ from near-fault strong-motion data. First, we replicated the results by F&M using 2D analysis of $S$-wave radiation from a kinematic-rupture description in a steady-state antiplane fault model. The results show the following: (1) for wave radiation from a cohesive-like slip-rate function, the parameter $D_c''$ remains invariant with distance from the fault, despite of the rapid attenuation of the fault breakdown periods $T_c$, and (2), for waves radiated from a noncohesive slip-rate function ($D_c = 0$), in which $D_c''$ values are expected

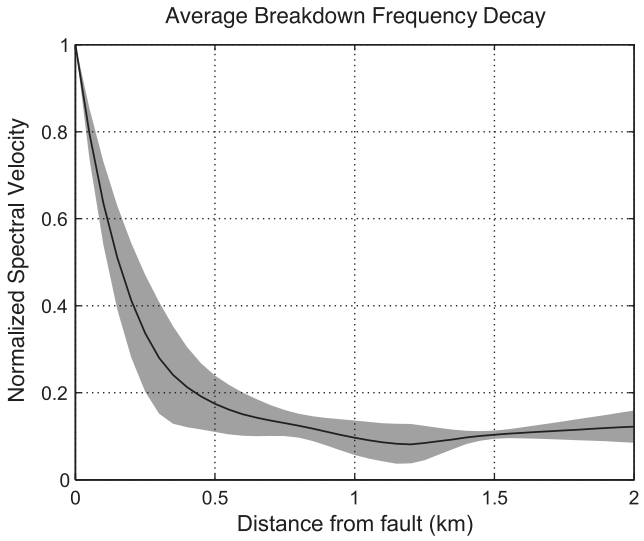


**Figure 18.** Attenuation of the average breakdown frequency ($f_c$, solid curve) and its standard deviation (gray band) along the five fault-perpendicular profiles depicted in Figure 17.

to be near zero, the $D_c''$ amplitude rapidly increases with distance. These results suggest that $D_c''$ is mainly controlled by wave propagation and rupture propagation effects, that are essentially unrelated to $D_c$.

Then we turn to more realistic tests based on 3D spontaneous ruptures reaching the Earth's surface and governed by a slip-weakening friction model. The results from these simulations suggest that $D_c''$ mainly depends on the value of the dynamic stress drop. We show that seismic energy related to the breakdown process decays very fast with distance from the fault, causing $D_c''$ to be rather insensitive to $D_c$. The simulations suggest that $D_c''$ measurements are essentially unrelated to $D_c$ beyond a narrow zone around the fault, which we refer to as the resolution zone for $D_c$. The width of this zone, $R_c$, is case dependent because it is a function of the breakdown frequencies. Our numerical experiments suggest that $R_c$ is on the order of a few hundreds of meters for relatively smooth ruptures and possibly up to about 1.5 km for more heterogeneous sources. Thus, our results show that the $D_c''$ parameter proposed by F&M may be related to the breakdown slip $D_c$ only within the resolution zone, which is considerably smaller than what their results suggest.

We estimate $R_c$ using two different approaches, described in the following manner. (1) $R_c$ is estimated as approximately equal to 80% of the wavelength associated with the breakdown frequency $f_c$ (i.e., the inverse of the dynamic stress-drop time span, also called breakdown period $T_c$). As a consequence, $R_c$ is case dependent and can only be estimated *a posteriori* for real earthquakes. (2) $R_c$ is estimated as the length of the cohesive zone $\Lambda_c$ over a small observable fault patch. Beyond $R_c$, $D_c''$ is entirely governed by the dynamic stress drop without any information of $D_c$. Furthermore, for ruptures reaching the Earth's surface and at distances from the fault less than $R_c$, the technique introduced by F&M overestimates $D_c$ approximately by a factor of 2 due to the omission of the free-surface amplification in their procedure.

F&M used their technique to estimate $D_c$ for the 2000 $M_w$ 6.6 Tottori and 2002 $M_w$ 7.9 Denali earthquakes as 0.3 and 2.5 m, respectively. The estimate for the Denali earthquake is done using strong-motion data recorded 3 km from the fault, at Pump Station 10 (PS10). If we consider reported breakdown periods for the 2002 Denali earthquake by Aagaard *et al.* (2004), for which $T_c < 0.5$ sec and $V_S = 3.4$ km/sec as the average near-surface $S$-wave velocity, then $R_c$ estimated from $f_c$ is less than 1.4 km. In other words, a subshear rupture pulse from the Denali earthquake would not contain sufficient information from the breakdown process for $D_c$ to be estimated at PS10. However, the most prominent pulse recorded at PS10 has been identified by some authors as a shock wave excited during a supershear rupture transient (e.g., Dunham and Archuleta, 2004). Because our findings about $R_c$ are related to subshear rupture propagation only, further study is needed to validate the estimate of $D_c$ at PS10 for the Denali earthquake by F&M. In the case of the Tottori earthquake, generally considered a subshear event, F&M estimated $D_c$ using the strong-motion data recorded at station GSH, which is located only about 100 m from the surface fault projection. However, according to geological observations, Semmane *et al.* (2005) have demonstrated that no coseismic surface rupture was observed for that earthquake. Our numerical tests, supported by near-fault strong-motion records of the 2004 Parkfield earthquake, show that if a vertical strike-slip rupture stops a few hundred meters below the Earth's surface, $D_c''$ does not contain any information about $D_c$. Thus, the $D_c''$ value determined by F&M for the Tottori earthquake is likely unrelated to the breakdown slip $D_c$ on the fault.

Finally, our results strongly question the reliability of $D_c$ estimates obtained from kinematic-rupture inversion using bandlimited strong-motion data. Such studies usually include strong-motion data recorded at distances of tens or hundreds of kilometers from the fault (e.g., Ide and Takeo, 1997). The resolution of $D_c$ must be evaluated based on event-specific estimates of $R_c$, fault complexity, and whether rupture propagated with subshear or supershear speed. However, the narrow $R_c$ zones consistently obtained from our simulations suggest that $D_c$ estimates from strong-motion source inversions are likely to be strongly influenced by wave propagation effects in most cases, in agreement with studies by Guatteri and Spudich (2000) and Spudich and Guatteri (2004).

## Data and Resources

All simulations were done on the DataStar and BlueGene computing clusters of the San Diego Supercomputer Center. Seismograms of the 2004 Parkfield earthquake were collected from the database of the Consortium of Organizations for Strong Motion Observation Systems (COSMOS). Data can be obtained from the COSMOS Virtual Data

Centre at http://www.cosmos-eq.org/ (last accessed November 2008).

## Acknowledgments

We are grateful to Elisa Tinti for providing the routine to generate regularized slip-rate Yoffe functions, as well as to Eric Dunham, Steven Day, James Rice, and Yuri Fialko for constructive and very fruitful discussions. Our manuscript was improved by reviews from Ben Duan and an unknown referee.

## References

Aagaard, B. T., G. Anderson, and K. W. Hudnut (2004). Dynamic rupture modeling of the transition from thrust to strike-slip motion in the 2002 Denali fault earthquake, Alaska, *Bull. Seismol. Soc. Am.* **94,** S190–S201.

Aki, K., and P. G. Richards (2002). *Quantitative Seismology*, Second Ed., University Science Books, Sausalito, California, 700 pp.

Anderson, J. G., and J. E. Luco (1983). Parametric study of near-field ground motion for a strike-slip dislocation model, *Bull. Seismol. Soc. Am.* **73,** 23–43.

Andrews, D. J. (1976). Rupture velocity of plane-strain shear cracks, *J. Geophys. Res.* **81,** 5679–5687.

Andrews, D. J. (2005). Rupture dynamics with energy loss outside the slip zone, *J. Geophys. Res.* **110,** B01307, doi 10.1029/2004JB003191.

Cruz-Atienza, V. M., and J. Virieux (2004). Dynamic rupture simulation of non-planar faults with a finite-difference approach, *Geophys. J. Int.* **158,** 939–954.

Cruz-Atienza, V. M., J. Virieux, and H. Aochi (2007). 3D finite-difference dynamic-rupture modelling along non-planar faults, *Geophysics* **72,** SM123, doi 10.1190/1.2766756.

Dalguer, L. A., and S. Day (2007). Staggered-grid split-node method for spontaneous rupture simulation, *J. Geophys. Res.* **112,** B02302, doi 10.1029/2006JB004467.

Dalguer, L. A., S. M. Day, K. B. Olsen, and V. M. Cruz-Atienza (2008). Rupture models and ground motion for Shakeout and other southern San Andreas fault scenarios, *14th World Conf. on Earthquake Engineering*, October 12–17, Beijing, China.

Dalguer, L. A., K. Irikura, W. Zhang, and J. Riera (2002). Distribution of dynamic and static stress changes during 2000 Tottori (Japan) earthquake: Brief interpretation of the earthquake sequences; foreshocks, main shock and aftershocks, *Geophys. Res. Lett.* **29,** no. 16, 1758, doi 10.1029/2001GL014333.

Day, S. M. (1982). Three-dimensional simulation of spontaneous rupture: The effect of nonuniform prestress, *Bull. Seismol. Soc. Am.* **72,** 1881–1902.

Day, S. M., L. A. Dalguer, N. Lapusta, and Y. Liu (2005). Comparison of finite difference and boundary integral solutions to three-dimensional spontaneous rupture, *J. Geophys. Res.* **110,** B12307, http://dx.doi.org/10.1029/2005JB003813.

Dieterich, J. H. (1979). Modelling of rock friction 1. Experimental results and constitutive equations, *J. Geophys. Res.* **84,** 2161–2168.

Dunham, E. M., and R. J. Archuleta (2004). Evidence for a supershear transient during the 2002 Denali fault earthquake, *Bull. Seismol. Soc. Am.* **94,** S256–S268.

Dunham, E. M., and R. J. Archuleta (2005). Near-source ground motion from steady state dynamic rupture pulses, *Geophys. Res. Lett.* **32,** L03302, doi 10.1029/2004GL021793.

Fukuyama, E., and T. Mikumo (2007). Slip-weakening distance estimated at near-fault stations, *Geophys. Res. Lett.* **34,** L09302, doi 10.1029/2006GL029203.

Fukuyama, E., T. Mikumo, and K. B. Olsen (2003). Estimation of the critical slip-weakening distance: Theoretical background, *Bull. Seismol. Soc. Am.* **93,** 1835–1840.

Gottschaemmer, E., and K. B. Olsen (2001). Accuracy of the explicit planar free-surface boundary condition implemented in a fourth-order staggered-grid velocity-stress finite-difference scheme, *Bull. Seismol. Soc. Am.* **91,** 617–623.

Guatteri, M., and P. Spudich (2000). What can strong motion data tell us about slip-weakening fault-friction laws?, *Bull. Seismol. Soc. Am.* **90,** 98–116.

Harris, R. A., M. Barall, R. Archuleta, E. Dunham, B. Aagaard, J. P. Ampuero, H. Bhat, V. M. Cruz-Atienza, L. Dalguer, P. Dawson, S. Day, B. Duan, G. Ely, Y. Kaneko, Y. Kase, N. Lapusta, Y. Liu, S. Ma, D. Oglesby, K. Olsen, A. Pitarka, S. Song, and E. Templeton (2009). The SCEC/USGS dynamic earthquake-rupture code verification exercise, Seism. Res. Lett. **80,** no. 1, 119–126, doi 10.1785/gssrl.80.1.119.

Ida, Y. (1972). Cohesive force across the tip of a longitudinal-shear crack and Griffith's specific surface energy, *J. Geophys. Res.* **77,** 3796–3805.

Ide, S., and M. Takeo (1997). Determination of constitutive relations of fault slip based on seismic waves analysis, *J. Geophys. Res.* **102,** 27,379–27,391.

Kostrov, B. V. (1964). Self-similar problems of propagation of shear cracks, *J. Appl. Math. Mech.* **28,** 1077–1087.

Liu, P., S. Custodio, and R. J. Archuleta (2006). Kinematic inversion of the 2004 *M* 6.0 Parkfield earthquake including an approximation to site effects, *Bull. Seismol. Soc. Am.* **96,** S143–S158, doi 10.1785/0120050826.

Ma, S., S. Custodio, R. J. Archuleta, and P. Liu (2008). Dynamic modeling of the 2004 $M_w$ 6.0 Parkfield, California, earthquake, *J. Geophys. Res.* **113,** B02301, doi 10.1029/2007JB005216.

Madariaga, R. (1978). The dynamic field of Haskell's rectangular dislocation fault model, *Bull. Seismol. Soc. Am.* **68,** 869–887.

Madariaga, R., K. B. Olsen, and R. Archuleta (1998). Modeling dynamic rupture in a 3D earthquake fault model, *Bull. Seismol. Soc. Am.* **88,** 1182–1197.

Mai, P. M., and G. C. Beroza (2002). A spatial random field model to characterize complexity in earthquake slip, *J. Geophys. Res.* **107,** no. B11, 2308, doi 10.1029/2001JB000588.

Marcinkovich, C., and K. Olsen (2003). On the implementation of perfectly matched layers in a three-dimensional fourth-order velocity-stress finite difference scheme, *J. Geophys. Res.* **108,** no. B5, 2276, doi 10.1029/2002JB002235.

Matsu'ura, M., H. Kataoka, and B. Shibazaki (1992). Slip-dependent friction law and nucleation processes in earthquake rupture, *Tectonophysics* **211,** 135–148.

Mikumo, T., and Y. Yagi (2003). Slip-weakening distance in dynamic rupture of in-slab normal-faulting earthquakes, *Geophys. J. Int.* **155,** 443–455.

Mikumo, T., K. B. Olsen, E. Fukuyama, and Y. Yagi (2003). Stress-breakdown time and slip-weakening distance inferred from slip velocity functions on earthquake faults, *Bull. Seismol. Soc. Am.* **93,** 264–282.

Miyatake, T., Y. Yagi, and T. Yasuda (2004). The dynamic rupture process of the 2001 Geiyo, Japan, earthquake, *Geophys. Res. Lett.* **31,** L12612, doi 10.1029/2004GL019721.

Oglesby, D. D., R. J. Archuleta, and S. B. Nielsen (2000). The three-dimensional dynamics of dipping faults, *Bull. Seismol. Soc. Am.* **90,** 616–628, doi 10.1785/0119990113.

Ohnaka, M., and T. Yamashita (1989). A cohesive fault model for dynamic shear faulting based on experimentally inferred constitutive relation and strong motion source parameters, *J. Geophys. Res.* **94,** 4089–4104.

Ohnaka, M., Y. Kuwahara, and K. Yamamoto (1987). Constitutive relations between dynamic physical parameters near a tip of the propagating slip zone during stick-slip shear failure, *Tectonophysics* **144,** 109–125.

Olsen, K. B. (1994). Simulation of three-dimensional wave propagation in the Salt Lake Basin, *Ph.D. Thesis*, University of Utah.

Olsen, K. B., S. M. Day, L. A. Dalguer, J. Mayhew, Y. Cui, J. Zhu, V. M. Cruz-Atienza, D. Roten, P. Maechling, T. H. Jordan, D. Okaya, and A. Chourasia (2009). ShakeOut-D: Ground motion estimates using an ensemble of large earthquakes on the southern San Andreas

fault with spontaneous rupture propagation, *Geophys. Res. Lett.* **36,** L04303, doi 10.1029/2008GL036832.

Olsen, K. B., R. Madariaga, and R. J. Archuleta (1997). Three-dimensional dynamic simulation of the 1992 Landers earthquake, *Science* **278,** 834–838.

Palmer, A., and J. R. Rice (1973). The growth of slip surfaces in the progressive failure of over-consolidated clay, *Proc. Roy. Soc. London, Ser. A* **332,** 527–548.

Peyrat, S., K. B. Olsen, and R. Madariaga (2001). Dynamic modeling of the 1992 Landers earthquake, *J. Geophys. Res.* **106,** 26,467–26,482.

Piatanesi, A., E. Tinti, M. Cocco, and E. Fukuyama (2004). The dependence of traction evolution on the earthquake source time function adopted in kinematic rupture models, *Geophys. Res. Lett.* **31,** L04609, doi 10.1029/2003GL019225.

Pulido, N., and K. Irikura (2000). Estimation of dynamic rupture parameters from the radiated seismic energy and apparent stress, *Geophys. Res. Lett.* **27,** 3945–3948.

Roten, D., K. B. Olsen, H. Magistrale, J. C. Pechmann, and V. M. Cruz-Atienza (2009). 3-D ground motion modeling for *M* 7 dynamic rupture earthquake scenarios on the Wasatch fault, Utah, *Seismological Society of America Annual Meeting*, 8–10 April, Monterey, California.

Ruina, A. (1983). Slip instability and state variable friction laws, *J. Geophys. Res.* **88,** 10,359–10,370.

Rymer, M. J., J. C. Tinsley, J. A. Treiman, J. R. Arrowsmith, K. B. Clahan, A. M. Rosinski, W. A. Bryant, H. A. Snyder, G. S. Fuis, N. Toké, and G. W. Bawden (2006). Surface fault slip associated with the 2004 Parkfield, California, earthquake, *Bull. Seismol. Soc. Am.* **96,** S11–S27.

Semmane, F., F. Cotton, and M. Campillo (2005). The 2000 Tottori earthquake: A shallow earthquake with no surface rupture and slip properties controlled by depth, *J. Gephys. Res.* **110,** B03306, doi 10.1029/2004JB003194.

Spudich, P., and M. Guatteri (2004). The effect of bandwidth limitations on the inference of earthquake slip-weakening distance from seismograms, *Bull. Seismol. Soc. Am.* **94,** 2028–2036.

Tinti, E., E. Fukuyama, A. Piatanesi, and M. Cocco (2005). A kinematic source-time function compatible with earthquake dynamics, *Bull. Seismol. Soc. Am.* **95,** 1211–1223.

Virieux, J., and R. Madariaga (1982). Dynamic faulting studied by a finite difference method, *Bull. Seismol. Soc. Am.* **72,** 345–369.

Yasuda, T., Y. Yagi, T. Mikumo, and T. Miyatake (2005). A comparison between $D_c'$-values obtained from a dynamic rupture model and waveform inversion, *Geophys. Res. Lett.* **32,** L14316, doi 10.1029/2005GL023114.

Zhang, W., T. Iwata, K. Irikura, H. Sekiguchi, and M. Bouchon (2003). Heterogeneous distribution of the dynamic source parameters of the 1999 Chi-Chi, Taiwan, earthquake, *J. Geophys. Res.* **108,** 2232, doi 10.1029/2002JB001889.

Universidad Nacional Autónoma de México
Instituto de Geofísica, Departamento de Sismología
Circuito de la Investigación Científica s/n
Ciudad Universitaria, 04510, México D.F.
cruz@geofisica.unam.mx
(V.M.C.)

Department of Geological Sciences
GMCS 231 MC-1020 5500 Campanile Drive
San Diego State University
San Diego, California 92182-1020
kbolsen@sciences.sdsu.edu
(K.B.O.)

Swiss Seismological Service
ETH-Zurich
CH-8093 Zurich, Switzerland
dalguer@tomo.ig.erdw.ethz.ch
(L.A.D.)

Manuscript received 14 November 2008